Tellus
SERIES B
CHEMICAL
AND PHYSICAL
METEOROLOGY
PUBLISHED BY THE INTERNATIONAL METEOROLOGICAL INSTITUTE IN STOCKHOLM

Tellus (2010), 62B, 770–783

Pulsed airborne lidar measurements of atmospheric CO_2 column absorption

By JAMES B. ABSHIRE[1]*, HARIS RIRIS[1], GRAHAM R. ALLAN[2], CLARK J. WEAVER[3], JIANPING MAO[3], XIAOLI SUN[1], WILLIAM E. HASSELBRACK[2], S. RANDOPH KAWA[1] and SEBASTIEN BIRAUD[4], [1]*NASA Goddard Space Flight Center, Greenbelt, MD 20771, USA;* [2]*Sigma Space Inc., Lanham, MD 20706, USA;* [3]*Goddard Earth Sciences and Technology Center, University of Maryland Baltimore County, Baltimore, MD 21228, USA;* [4]*Lawrence Berkeley National Laboratory, Berkeley, CA 94720, USA*

(Manuscript received 29 December 2009; in final form 22 July2010)

ABSTRACT

We report initial measurements of atmospheric CO_2 column density using a pulsed airborne lidar operating at 1572 nm. It uses a lidar measurement technique being developed at NASA Goddard Space Flight Center as a candidate for the CO_2 measurement in the Active Sensing of CO_2 Emissions over Nights, Days and Seasons (ASCENDS) space mission. The pulsed multiple-wavelength lidar approach offers several new capabilities with respect to passive spectrometer and other lidar techniques for high-precision CO_2 column density measurements. We developed an airborne lidar using a fibre laser transmitter and photon counting detector, and conducted initial measurements of the CO_2 column absorption during flights over Oklahoma in December 2008. The results show clear CO_2 line shape and absorption signals. These follow the expected changes with aircraft altitude from 1.5 to 7.1 km, and are in good agreement with column number density estimates calculated from nearly coincident airborne in-situ measurements.

1. Introduction

Atmospheric CO_2 is presently understood as the largest anthropogenic forcing function for climate change, but there is considerable uncertainty about the global CO_2 budget. Accurate measurements of tropospheric CO_2 abundances are needed to study CO_2 exchange with the land and oceans. To be useful in reducing uncertainties about carbon sources and sinks the atmospheric CO_2 measurements need to have high resolution, with $\sim 0.3\%$ precision (Tans et al., 1990; Fan et al., 1998). The GOSAT mission (Yokota et al., 2004) is making new global CO_2 measurements from space using a passive spectrometer and surface reflected sunlight. However sun angle limitations restrict its measurements to the daytime primarily over mid-latitudes. A concern for measurement accuracy with passive instruments is optical scattering from thin clouds in the measurement path (Mao and Kawa, 2004; Aben et al., 2007). Optical scattering in the measurement path modifies the optical path length and thus the total CO_2 absorption viewed by the instrument. For measurements using spectrometers with reflected sunlight optical scattering can cause large retrieval errors even for thin cirrus clouds (Uchino et al., 2009).

To address these issues, the US National Research Council's 2007 Decadal Survey for Earth Science recommended a new space-based CO_2 measuring mission called Active Sensing of CO_2 over Nights, Days, and Seasons, or ASCENDS (US NRC, 2007). The goals of the ASCENDS mission are to produce global atmospheric CO_2 measurements with much smaller seasonal, latitudinal, and diurnal biases by using the laser absorption spectroscopy measurement approach. The mission's goals are to quantify global spatial distribution of atmospheric CO_2 with 1–2 ppm accuracy, and quantify the global spatial distribution of terrestrial and oceanic sources and sinks of CO_2 on 1-degree grids with 2–3 week time resolution. The ASCENDS approach offers continuous measurements over the cloud-free oceans, at low sun angles and in darkness, which are major improvements over passive sensors. ASCENDS mission organizers held a workshop in 2008 to better define the science and measurement needs and planning for future work (NASA, 2008). ESA has also conducted mission definition studies for a similar space mission called A-SCOPE (ESA, 2008; Durand et al., 2009). Although the ASCENDS mission concept requires

*Corresponding author.
e-mail: James.B.Abshire@nasa.gov
DOI: 10.1111/j.1600-0889.2010.00502.x

a simultaneous dry air column measurement, the A-SCOPE mission concept does not. The lidar sensitivity and spectroscopic analyses performed as part of the A-SCOPE definition activities have been recently published (Ehret et al., 2008; Caron and Durand, 2009).

2. Candidate lidar approach for ASCENDS

NASA Goddard Space Flight Center has been developing a pulsed lidar approach for the measurement of atmospheric CO_2 concentrations as a candidate for the ASCENDS mission (Abshire et al., 2001, 2007; Riris et al., 2007). The approach uses a dual band pulsed laser absorption spectrometer and the integrated path differential absorption (IPDA) lidar technique (Measures, 1992). The instrument concept uses two tunable pulsed laser transmitters allowing simultaneous measurement of the absorption from a CO_2 absorption line in the 1570 nm band, O_2 absorption in the oxygen A-band, and surface height and atmospheric backscatter in the same path. A tunable laser is stepped in wavelength across a single CO_2 line for the CO_2 column measurement, while simultaneously a laser is stepped across a pair of lines near 765 nm in the Oxygen A-band for an atmospheric pressure measurement (Stephen et al., 2007, 2008). Both lasers are pulsed at a $\sim$8 kHz rate, and the two absorption line regions are repeatedly sampled at typically $\sim$1 kHz. Both laser transmitters utilize tunable diode lasers followed by laser fibre amplifiers. The direct detection receiver measures the time resolved laser backscatter from the atmosphere and the surface. After suitable averaging, the gas extinction and column densities for the CO_2 and O_2 gases are estimated from the sampled wavelengths of the surface reflected line shapes via the IPDA technique.

This approach measures the CO_2 lineshape at several spectrally resolved points, which provides several capabilities. This allows calculating atmospheric weighting functions at two to three heights (Mao et al., 2007). Sampling at multiple wavelengths across the absorption line allows for solving for wavelength offsets via a line fitting process. The distributed wavelength sampling across the line region also allows the instrument's response to be characterized as a function of wavelength. These capabilities allow modelling and reducing the impacts of wavelength dependent responses in the lidar. Using pulsed lasers and a time resolved receiver also allows post detection signal processing to isolate the laser echo signals from the surface, and to reject laser photons scattered from the atmosphere which arrive earlier. Hence it allows isolating the full column measurement from bias errors caused by atmospheric scattering (Mao and Kawa, 2004; Aben et al., 2007). The time gate used in the receiver processing also substantially improves the receiver's signal-to-noise ratio (SNR) by reducing the amount of noise included from the detector and solar background. This paper describes an initial airborne demonstration of the CO_2 column measurement using this technique.

3. Previous lidar measurements of CO_2

Several groups have measured atmospheric CO_2 absorption using DIAL lidar techniques. Researchers have reported lidar measurements using the CO_2 absorption lines in the 2051–2062 nm region using coherent detection. Phillips et al. (2004) describe a compact dual wavelength continuous wave (CW) laser absorption spectrometer designed for airborne integrated path measurements using a CO_2 line at 2051 nm and a receiver using coherent detection. Koch et al. (2004) have developed and demonstrated a ground-based range-resolved CO_2 backscatter profiling lidar, using a CO_2 line near 2050 nm, a pulsed Ho:Tm:YLF laser and a coherent receiver. They demonstrated CO_2 absorption measurements to within a few percent to a range of 3 km. Subsequently Koch et al. (2008) demonstrated an increase in laser power and vertical profiling of CO_2 near a CO_2 measuring tower. Gibert et al. (2006) have developed and demonstrated a ground based range resolved CO_2 backscatter profiling lidar, operating at a line near 2062 nm, based on a pulsed Ho:Tm:YLF laser and using a coherent receiver. They demonstrated CO_2 absorption measurements over horizontal path lengths of 2 km. Subsequently, Gibert et al. (2008) demonstrated and analysed numerous horizontal, slant path and vertical profiling measurements, as well as integrated path measurements to clouds.

Researchers have also reported lidar measurements using several different CO_2 lines in the 1570 nm CO_2 absorption band with direct detection receivers. Krainak et al. (2003) reported integrated path CO_2 absorption measurements over a 200-m horizontal path to a reflective target. Their lidar used a tunable CW laser, consisting of a wavelength scanned diode laser followed by erbium-doped fibre amplifier, to repeatedly sweep across the 1572.33 nm line. The direct detection receiver used a PIN photodiode detector. Riris et al. (2007), and Allan et al. (2008) describe the evolution of this lidar, its use for longer duration CO_2 absorption measurements over 0.4 and 1.6 km long horizontal paths, and comparison of its measurements with in situ sensor readings.

Amediek et al. (2008) reported on CO_2 measurements made using a lidar operating on the 1572.9 nm line, using a pulsed Optical Parametric Oscillator (OPO)-based laser transmitter, pumped by a Nd:YAG laser. Their direct detection receiver used a PIN photodiode detector. Integrated path CO_2 absorption measurements were made over a 2-km-long horizontal path to the sides of a tree stand and compared to an in situ sensor. Sakaizawa et al. (2009) reported on a ground-based backscatter profiling lidar using a Nd:YAG laser pumped OPO transmitter, a CO_2 line near 1572 nm, and a direct detection receiver using a photomultiplier (PMT) detector. They report measuring height resolved CO_2 absorption profiles to 5 km, and relative errors of 1% at $<$7 km height. Kameyama et al. (2009) have developed a dual wavelength sine-wave modulated CW lidar for integrated path CO_2 measurements. It used the 1572.9 nm line, an 11 cm diameter receiver and a PIN photodiode detector. They report CO_2

absorption measurements over a 1 km long horizontal path with 4 ppm fluctuations.

Several researchers have recently reported on airborne lidar relevant to CO_2 measurements. Amediek et al. (2009) have made airborne measurements of ground and water reflectance at 1573 nm in a set of flights over western Europe. Their lidar used a broadband OPO transmitter and a PIN photodiode detector and made normalized backscattered pulse energy measurements from 1.7 to 3 km altitudes. Browell et al. (2009) have been making measurements with an airborne lidar measuring integrated path CO_2 absorption from the aircraft to the surface. Their lidar uses a CO_2 line near 1571 nm, two CW fibre lasers whose powers are sine-wave modulated at different frequencies, and a direct detection receiver using lock-in detection for each modulation frequency. They reported good agreement with CO_2 values measured with in situ sensors on a number of flights to 7.5 km altitudes.

4. Airborne lidar measurement approach

We report here on the initial airborne measurements of CO_2 column density made with a pulsed lidar using the IPDA technique, a wavelength tunable laser with a fibre amplifier, and a direct detection photon counting receiver. The IPDA technique is a well-established technique for open-path laser absorption spectroscopy measurements (Measures, 1992; Weitkamp, 2005). It is essentially a special case of differential absorption lidar, where a scattering target (such as the ground, a water surface, trees, and cloud tops) is used at the end of the path. Typically two laser wavelengths are used, which have linewidths much narrower than the gas absorption line. The target is illuminated with the laser alternatively tuned onto the gas absorption line, and off it, at a nearby region. The path-integrated gas absorption attenuates the on-line laser energy relative to the off-line wavelength. By measuring the optical depth of the gas absorption line, and by knowing the difference in gas absorption cross-sections and path length, one can solve for the path integrated gas number density.

Our lidar uses a pulsed narrow linewidth laser, based on a tunable diode laser and fibre amplifier, which is repeatedly step-scanned in wavelength across the selected CO_2 absorption line. Twenty wavelength steps were used for these flights and the wavelength step size and other lidar parameters are summarized in Table 1. The receiver records and accumulates the backscattered photon counting profiles for the scan during the integration time. This contains the range resolved backscatter from any clouds or aerosols in the path as well as the surface echo pulses at each wavelength.

The quality of the lidar measurement depends on its signal and noise characteristics and the magnitude of bias errors. A detailed analysis must account for many factors, including variability in the lidar parameters, atmospheric temperature and pressure, turbulence, laser speckle, changing surface reflectivity and range,

Table 1. 2008 airborne lidar parameters

CO_2 line center wavelength	1572.33 nm
Laser min & max wavelengths	1572.29 nm, 1572.39 nm
Laser wavelength steps across line	20 (these flights)
Laser wavelength change/step	~5 pm
Laser peak power, pulse width	25 watts, 1 μsec
Laser pulse energy	25 μJ
Laser divergence angle	470 μrad (these flights)
Seed laser diode type	DFB: Fitel FOL15DCWD
Laser Pulse Modulator (AOM)	NEOS Model: 26035–2-155
Fiber coupled CO_2 cell	80 cm path, ~200 Torr pressure
Fiber Laser Amplifier (EDFA)	IPG EAR-10K-1571-LP-SF
Laser line scan rate	450 Hz
Laser linewidth per step	~15 MHz
Receiver Telescope type	Cassegrain, f/10 (Vixen)
Telescope diameter	20 cm
Receiver FOV diameter	200 μrad
Receiver optical bandwidth	800 pm FWHM
Receiver optics transmission (incl laser loss overfilling FOV)	16%
Detector type	PMT: Hamamatsu H10330A-75
Detector quantum efficiency	2% (this device)
Detector dark count rate	~325 kHz
Receiver signal processing	Photon counting/histogramming
Histogram time bin width	64 nsec (these flights)
Receiver integration time	1 s per readout
Recording duty cycle	50% (1 s every 2 s)
Instrument rack size & mass:	~90 cm tall, total: 147 kg
Sensor head size and mass	~25 × 60 × 60 cm, 41 kg

etc. (see Ehret et al., 2008 and Caron and Durand, 2009). The following is a simplified treatment for this approach for an open atmospheric path and target at a fixed range R, which illustrates some of the important dependencies. The measurement's signal and noise are determined from the lidar equations. The average signal detected at a measurement wavelength for a single laser pulse is given by

$$N_{\mathrm{sig}}(\lambda) = \eta_{\mathrm{det}} \frac{E_{\mathrm{las}}(\lambda)}{hc/\lambda} \frac{r_{\mathrm{sl}}}{\pi} \frac{A_{\mathrm{rcvr}}}{R^2} \tau_{\mathrm{opt}}(\lambda) \tau_{\mathrm{atm}}^2(\lambda). \quad (1)$$

The total detector noise counts within the laser pulse period, caused by detected reflected sunlight and detector dark noise, is

$$N_{\mathrm{n}} \approx \eta_{\mathrm{det}} \frac{I_{\mathrm{sol}}}{hc/\lambda} \Delta\lambda_{\mathrm{BPF}} \left(\frac{\theta_{\mathrm{FOV}}}{2}\right)^2 \frac{r_{\mathrm{sb}}}{\pi} A_{\mathrm{rcvr}} \tau_{\mathrm{opt}}(\lambda) T_{\mathrm{p}} + \dot{N}_{\mathrm{d}} T_{\mathrm{p}}, \quad (2)$$

where η_{det} is the detector photon counting efficiency; $E_{\mathrm{las}}(\lambda)$ is the laser pulse energy at a given wavelength; h is the Planck's constant; c is the speed of light; λ is the laser wavelength; r_{sl} is the target surface's effective diffuse reflectivity to the laser signal; r_{sb} is the target surface's effective diffuse reflectivity to sunlight in the receiver's line-of-sight; A_{rcvr} is the collecting area of receiver telescope; R is the range from the instrument to the surface; $\tau_{\mathrm{opt}}(\lambda)$ is the receiver optical transmission at a given wavelength; $\tau_{\mathrm{atm}}(\lambda)$ is the one-way atmosphere transmission at the laser wavelength; I_{sol} is the solar spectral irradiance; $\Delta\lambda_{\mathrm{BPF}}$

is the receiver optical bandwidth; θ_{FOV} is the diameter of receiver field of view; $\dot{N}_{\mathrm{d}}$ is the detector dark noise count rate (Hz) and T_{p} is the receiver pulse integration time, usually slightly larger than the laser pulse width.

The two-way atmospheric transmission is a function of the laser wavelength. It is related to the total column CO_2 density by

$$\tau^2_{\mathrm{atm}}(\lambda) = \tau^2_{\mathrm{off}} \exp\left\{-2\int_0^R [\sigma(\lambda, r) - \sigma(\lambda_{\mathrm{off}}, r)]\, n_{\mathrm{CO_2}}(r)\, \mathrm{d}r\right\}, \tag{3}$$

where τ^2_{off} is the two-way atmosphere transmission, when the laser is tuned off the absorption line, $\sigma(\lambda, r)$ is the CO_2 molecular absorption cross-section at the laser wavelength λ and range r, $\sigma(\lambda_{\mathrm{off}}, r)$ is the offline CO_2 absorption cross-section, and $n_{\mathrm{CO_2}}(r)$ is the CO_2 molecular volume density.

For airborne measurements though a nadir (vertical) path, the pressure and temperature both change with r. The varying pressure and temperature change the line shape and causes $\sigma(\lambda, r)$ to vary with range, and hence cause an altitude dependence (or weighting) in absorption. However, for the simplest case, when the path's temperature and pressure conditions are approximately uniform, the line shape and cross-sections about constant along the path, so for it

$$\tau^2_{\mathrm{atm}}(\lambda) = \tau^2_{\mathrm{off}} \exp\left\{-2[\sigma(\lambda) - \sigma(\lambda_{\mathrm{off}})]\int_0^R n_{\mathrm{CO_2}}(r)\, \mathrm{d}r\right\}. \tag{4}$$

For this simpler case, and for using a single wavelength for the online measurement, the total column CO_2 abundance can be computed from the ratio of the numbers of the detected photons on- and off-line from the CO_2 absorption wavelength, as

$$\begin{aligned} R_{\text{on-off}} &\equiv \frac{N_{\mathrm{sig}}(\lambda_{\mathrm{on}})}{N_{\mathrm{sig}}(\lambda_{\mathrm{off}})}\frac{E_{\mathrm{las}}(\lambda_{\mathrm{off}})\tau_{\mathrm{opt}}(\lambda_{\mathrm{off}})}{E_{\mathrm{las}}(\lambda_{\mathrm{on}})\tau_{\mathrm{opt}}(\lambda_{\mathrm{on}})} \\ &= \exp\left\{-2[\sigma(\lambda_{\mathrm{on}}) - \sigma(\lambda_{\mathrm{off}})]\int_0^R n_{\mathrm{CO_2}}(r)\, \mathrm{d}r\right\} \end{aligned} \tag{5}$$

or

$$N_{\mathrm{CO_2}} \equiv \int_0^R n_{\mathrm{CO_2}}(r)\, \mathrm{d}r = \frac{-1}{2[\sigma(\lambda_{\mathrm{on}}) - \sigma(\lambda_{\mathrm{off}})]} \ln\left(R_{\text{on-off}}\right). \tag{6}$$

The optical depth of the line absorption is defined as - $\ln(R_{\mathrm{on-off}})$. Here we have defined $R_{\text{on-off}}$ as the ratio of the received signal photons measured for the on- and off-line wavelengths multiplied by a fraction, which depends on the lidar's wavelength response versus wavelength. Equation (5) assumes that the surface reflectivity r_{sl} is equal at both wavelengths. This is an approximation for a wavelength-stepped lidar measuring from a moving aircraft, particularly if the surface area (and reflectivity) viewed by the lidar changes at an appreciable fraction of the lidar's wavelength step rate (Amediek et al., 2009). However, as discussed in Section 8, it was a good approximation for these airborne measurements over nearly uniformly reflecting terrain, where there were usually several wavelength scans per illuminated measurement spot.

For measuring a uniform path with two wavelengths, the fractional error in the average column CO_2 measurement error can be approximated as

$$\varepsilon_N \equiv \frac{\delta(N_{\mathrm{CO_2}})}{N_{\mathrm{CO_2}}} \approx \frac{1}{\ln(R_{\text{on-off}})}\frac{\delta(R_{\text{on-off}})}{R_{\text{on-off}}}, \tag{7}$$

where $\delta(x)$ denotes the error in the measurements of x.

The random errors are due to the statistical uncertainties (finite signal-to-noise ratio) of the received signal. The fractional random error in the ratio of the net on- and off-line signal can be approximated as

$$\begin{aligned} \delta(R_{\text{on-off}}) &\approx \partial\left[\frac{N_{\mathrm{sig}}(\lambda_{\mathrm{on}})}{N_{\mathrm{sig}}(\lambda_{\mathrm{off}})}\right] \\ &= R_{\text{on-off}}\left\{\frac{-\partial[N_{\mathrm{sig}}(\lambda_{\mathrm{off}})]}{N_{\mathrm{sig}}(\lambda_{\mathrm{off}})} + \frac{\partial[N_{\mathrm{sig}}(\lambda_{\mathrm{on}})]}{N_{\mathrm{sig}}(\lambda_{\mathrm{on}})}\right\}. \end{aligned} \tag{8}$$

Hence, for this case, the standard deviation of the fraction error of the total column CO_2 number density due to random errors can be written as

$$\sigma_{\varepsilon N} = \frac{-1}{\ln(R_{\text{on-off}})}\left(\frac{1}{SNR_{\mathrm{off}}} + \frac{1}{SNR_{\mathrm{on}}}\right). \tag{9}$$

In general, for a direct detection lidar, the detected signal fluctuates from both speckle and shot noise. The speckle noise contribution can be estimated from λ, the laser beam divergence, and A_{rcvr} (Tsai and Gardner, 1985). For these experiments the number of speckle correlation cells captured by the receiver telescope per laser firing, K_{s} was ~6100, which was much larger than the detected number of signal photons per firing. Hence the speckle noise effects were negligible and the random errors were caused by shot noise in the signal and background. The signal-to-noise ratio at each wavelength, can be computed for each laser shot from

$$SNR_i = \frac{N_{\mathrm{tot}} - N_n}{\sqrt{N_{\mathrm{tot}} + N_n}} = \frac{N_{\mathrm{sig}}}{\sqrt{N_{\mathrm{sig}} + 2N_n}}, \tag{10}$$

where N_{tot}, N_n and N_{sig} are the total detected photons, the detected background and dark counts accumulated over the laser pulse width, and the detected signal photons, respectively, for that wavelength. Note that the receiver has to estimate the noise photon count separately, which can be done by integrating the detector output after the occurrence of the ground echo pulse.

After accumulating photon counts for an integration time T_{int}, the averaged signal-to-noise ratios in (9) at each wavelength are given by

$$SNR(\lambda) = \sqrt{f(\lambda)_{\mathrm{las}} T_{\mathrm{int}}}\, SNR_i, \tag{11}$$

where $f(\lambda)_{\mathrm{las}}$ is the laser pulse rate at wavelength λ and $f(\lambda)_{\mathrm{las}} T_{\mathrm{int}}$ is the total number of pulse measurements averaged. The total column CO_2 measurement error in abundance can be

obtained by multiplying $\sigma_{\varepsilon N}$ in (9) by the nominal CO_2 abundance.

Bias errors occur when there are errors in the mean values of the lidar and experiment parameters. For laser absorption spectrometers, including lidar based on the IPDA technique, there are many potential sources of bias errors. These include errors in line strengths from spectroscopy, errors in estimating the laser powers and wavelengths, errors in estimating R, non-linearities in detector response with power, etc. For these experiments the accuracy of the range (altimetry) measurement was estimated to be ∼5 m, and the relative error from path length errors was small. The linearity of the photon counting receiver used for these experiments is being evaluated.

A common error is from small changes (a few per cent or less) in the instrument 'baseline', that is, in the product $E_{\rm las}(\lambda)\,\tau_{\rm opt}(\lambda)$, versus wavelength in eq. (5). Ideally this product is a constant, but typically it varies with wavelength, and also changes with time and temperature. Variability in the baseline response with wavelength is usually the limiting error source in laser absorption spectrometers (Werle et al. 1993, 2004). However sampling the absorption line region at multiple wavelengths around the line allows the lidar's wavelength variability to be modelled, and the modelled values may be used in eq. (5). This approach can significantly reduce the error in $N_{\rm CO_2}$. More wavelength samples usually allows for more accurate modelling. However, with a fixed time delay between laser pulses, using more wavelength samples also slows the line scan rate. As the line scan rate is reduced, an airborne lidar becomes more sensitive to variability from surface reflectance changes, which introduce measurement errors. For these initial flights the dominant error source was the ∼8% variability in $\tau_{\rm opt}(\lambda)$ caused by etalon fringes (see for example, Hecht, 2000) from the aircraft's plane-parallel nadir window. For these flights we adjusted the lidar to sample the CO_2 line region at 20 wavelength samples, in order to allow about four wavelength samples per window etalon fringe period. This resulted in a 450 Hz line scan rate, and allowed modelling of window etalon fringe transmission from the measurements as part of the retrieval approach, which simultaneously solved for the line absorption depth and for the baseline response.

5. CO_2 spectroscopy and line choice

The near infrared vibration-rotation bands of CO_2 at 1.57, 1.6 and 2.1 μm have been recommended for remote sensing (Kuang et al., 2002; O'Brien and Rayner, 2002; Dufour and Breon, 2003; Mao and Kawa, 2004; Caron and Durand, 2009). We used a line in the 1570 nm band (Fig. 1) for the CO_2 measurement (Mao and Kawa, 2004). This vibration-rotation band of CO_2 has an appropriate range of absorption that provides good sensitivity to the surface echo signal and to variation in CO_2 in the lower troposheric column. This band has minimal interferences from other atmospheric species like H_2O, and has several

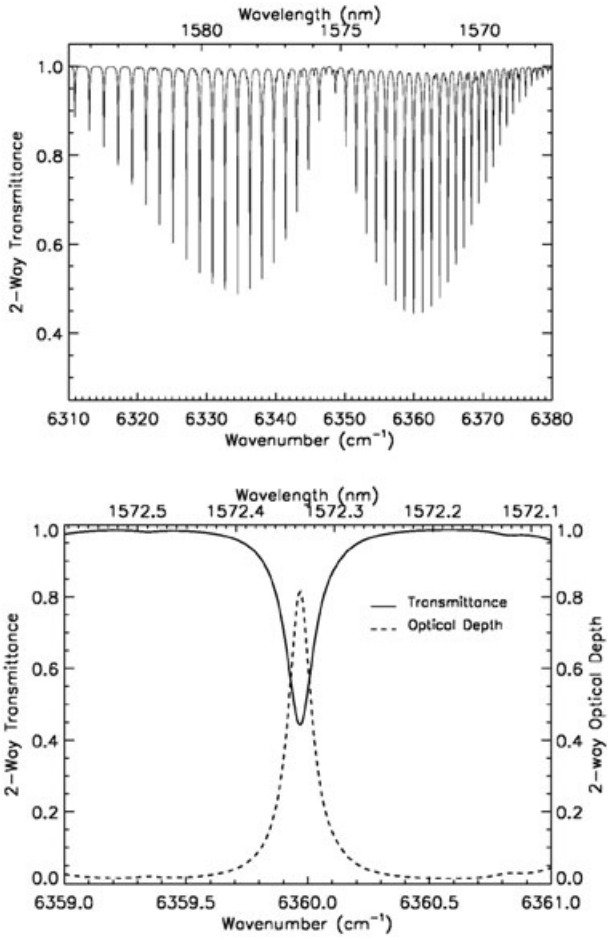

Fig. 1. Calculated CO_2 band absorption (top panel) and the 1572.335 nm line shape (bottom panel) calculated from HITRAN 2004 for two-way path from a 5 km aircraft altitude to ground, based on the US standard atmosphere. The line shape is plotted both in transmission (solid) and in optical depth (dashed).

different lines, which are sufficiently insensitive to changes in atmospheric temperature.

The shorter wavelength lines in the R-branch are a better match to available laser and detector technologies. The centre-line of R-branch at 1572.335 nm, shown in Fig. 1, has been analysed and recommended as an attractive line for CO_2 measurements (Mao et al., 2007). It has the minimum temperature sensitivity, particularly to the lower atmospheric temperature changes. It also provides the maximum CO_2 absorption in the R-branch. Absorption measurements on this line at a several different wavelengths yield the line shape and CO_2 vertical column densities with absorption weighting functions peaking at several different altitudes.

6. Airborne lidar description

We first developed a ground-based lidar to demonstrate CO_2 absorption measurements over horizontal paths to cooperative

Fig. 2. Top panel: NASA Glenn Lear-25 aircraft. The nadir window assembly is just below the NASA logo. Bottom panels: photograph of the lidar installed on the aircraft showing the sensor head assembly (left-hand panel) and the dual aircraft racks (right-hand panel).

targets. This lidar used a continuous-wave distributed feedback (DFB) diode laser, operating at a selected CO_2 line near 1572 nm, followed by an erbium doped fibre amplifier (EDFA). The laser wavelength was swept across the CO_2 line at KHz rates by tuning the current to the diode laser and the output was gated by a mechanical chopper. The receiver was a 20 cm diameter telescope and a PIN photodiode detector, followed by an analogue to digital converter. The ground based lidar was used to make long-term laboratory measurements of absorption from CO_2 in a cell, and in over open paths using cooperative targets. We also made field measurements of integrated path CO_2 absorptions over 0.2–1.6-km-long horizontal paths at two different sites (Riris et al., 2007; Allan et al., 2008).

We subsequently modified the ground-based instrument for use on the NASA Glenn Lear-25 aircraft shown in Fig. 2. A block diagram of the flight instrument (Abshire et al., 2009a) is shown in Fig. 3. Modifications to the ground based lidar included converting the laser transmitter to pulsed operation by adding an acousto-optic modulator (AOM) between the diode laser and the fibre amplifier, removing the chopper wheel, and improving the receiver sensitivity by using a PMT detector, followed by a discriminator and multichannel scaler (MCS). The airborne lidar specifications are listed in Table 1.

For the airborne instrument, the laser signal source is DFB laser diode, which is stabilized near 1572.33 nm by controlling its temperature and current. A voltage ramp from a signal generator was used to sweep the current to the diode laser, and hence its output wavelength. The diode's CW output is then gated into pulses using an acousto-optic modulator (AOM). The laser pulse timing is synchronized to the tuning of the laser wavelength so that the CO_2 absorption peak occurs in the middle of the scan. A small percentage of the CW seed laser output is split off and directed through a fibre-coupled CO_2 absorption cell and to a PIN detector. The CO_2 cell serves as a monitor for centre wavelength of the sweep. An initial calibration procedure was used on the ground to test and determine the wavelength of each of the transmitted laser pulses. This used a commercial wavemetre with 0.1 pm resolution to measure the wavelength of the diode laser as it was stepped through the nominal voltages of the ramp. Subsequent testing showed some curvature in the actual dynamic ramp signal, so a more accurate model of the laser wavelength versus pulse position was a quadratic function, which was used in data analysis.

The output of the transmitter is a sequence of 1 μs wide laser pulses every 100 μs (e.g. a 10 KHz pulse rate) as is shown in Fig. 4. The peak power was approximately 25 W. Each laser pulse contains about 25 μJ and over 90% of the pulse energy. A sample of the laser diode sweep through the internal cell containing CO_2 is shown in Fig. 5, along with a sample of the pulsed transmitter wavelength sweep. The optical power versus time waveform of a single pulse from the transmitter is shown in Fig. 6.

The collimated transmitted laser signal exits through the nadir aircraft window. The laser backscatter is collected by the receiver's 20 cm diameter Cassegrain telescope, which views nadir through the same window in a bistatic configuration. A multimode optical fibre is used to couple the optical signal from the telescope focal plane to the receiver optics. After passing

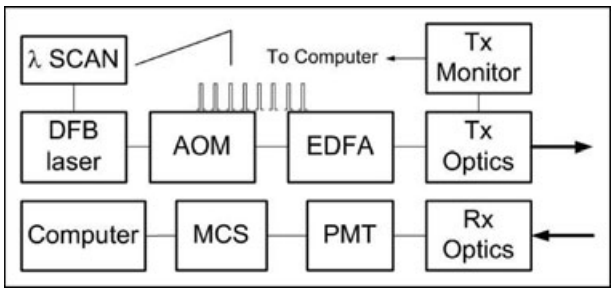

Fig. 3. Block diagram of the airborne lidar.

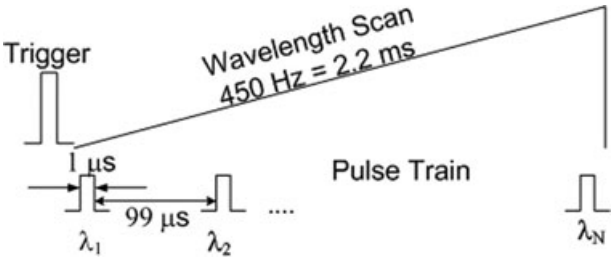

Fig. 4. Timing diagram of the laser pulse and wavelength sweep used to generate pulsed wavelength scans of CO_2 line. A wavelength scan with 20 pulses was used for the December 2008 flights.

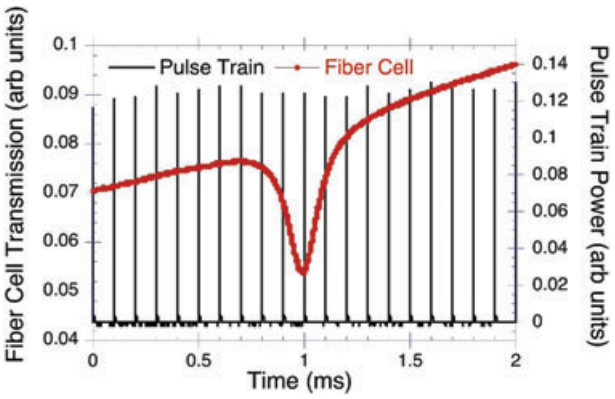

Fig. 5. Example of laser wavelength scan. (Red trace and left hand axis)—Sample cw wavelength scan of the diode laser (before the modulator) through the instrument's internal low pressure CO_2 cell, showing CO_2 absorption and diode laser power variability versus wavelength. (Black trace and right hand axis)—Detected laser power versus time from the laser transmitter's power monitor.

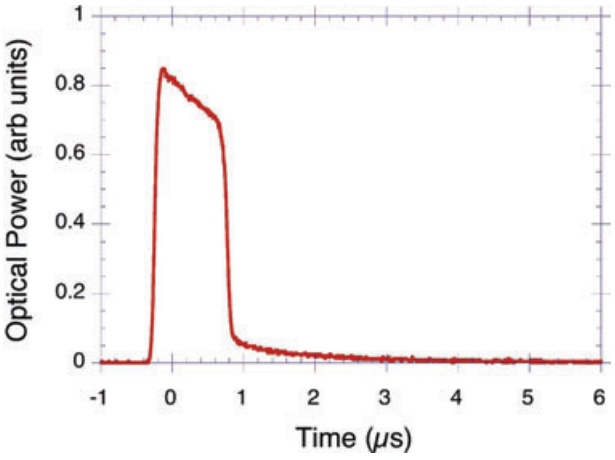

Fig. 6. Typical single laser pulse from the airborne laser transmitter. The pulse shape shows decay as the fibre amplifier gain is depleted. The 1 μs wide part of the laser pulse contains over 90% of the pulse energy.

through an optical bandpass filter, the signal is focused onto a PMT detector. The PMT has a single photon detection efficiency of ~2%. The electrical pulse output from the PMT was amplified and passed through a threshold detector.

The pulses from the discriminator are binned and accumulated by the MCS. One MCS sweep records all detected PMT pulses for the sequence of 20 laser pulses. The start time of the MCS sweep is synchronized with the first laser pulse trigger and hence start of the pulsed wavelength sweep. Each MCS sweep contains a histogram of PMT pulse counts versus time for the wavelength sweeps (i.e. the laser backscatter profiles for all 20 pulses). At the end of 1 s, each MCS bin contains the total receiver counts, at its respective time delay, for the 450 laser sweeps. The receiver histogram record is then read and stored. Due to the time required for the readout, data was stored every other second. The laser trigger and data acquisition is synchronized to timing markers from the GPS receiver. The computer also digitizes other signals, including those from eight thermocouples distributed across the sensor head and electronic rack, the inertial guidance system output from the aircraft and GPS position and time. A nadir viewing video camera also captures the visible image though the nadir window during flight.

7. Airborne campaigns

The NASA Glenn Lear-25 aircraft (NASA-Glenn, 2010) was selected for these flights based on maximum altitude capability. For work related to space missions, it is important to provide a high altitude path, which includes expected effects such as scattering from cirrus clouds. The airborne CO_2 lidar was integrated onto the Lear-25 in early October 2008 for two engineering flights. The airborne lidar was configured into two half-racks and a 'sensor head', which contained the receiver telescope and the transmitter optics. A photograph of the sensor when integrated on the aircraft is shown in Fig. 2.

The sensor head was mounted above the aircraft's nadir viewing window. The original design called for antireflection (AR) coated, wedged optical windows to be used. However, due to window delivery delays, these first flights were performed with the aircraft's standard quartz nadir camera window.

The experiment team flew six flights over Ohio and Oklahoma during October and December 2008. Each flight lasted just over 2 h, which was limited by the aircraft's fuel capacity. These flights allowed testing and recording performance under different measurement conditions. These included measuring to the ground through broken and thin clouds. An example of these measurements is shown in Fig. 7. It shows the time resolved double-echo pulses measured when viewing the ground over the DOE ARM site at 7.2 km altitude through thin clouds ~1 km below the aircraft. The first pulse in each pair is the reflection from the cloud, while the second is reflection from the ground. Without range gating, the echo pulse signals and measurements from the two different path lengths are mixed. Using the pulsed measurement approach allows using range gating in the data processing to isolate the signal from the surface and eliminates optical path length errors from cloud scattering.

The earlier flights also illustrated the impact of the wavelength variability introduced by the etalon fringes from the aircraft's uncoated plane-parallel nadir window. The raw CO_2 absorption line shape measurements were distorted by the ±4% transmission variability caused by etalon fringes from the window. These were approximately sinusoidal with ~4 cycles across the sweep. These changed with time and temperature and caused $\tau(\lambda)_{opt}$ to vary in flight. On these flights this variability limited our capability to estimate the CO_2 line shape and absorbance. For subsequent flights (Abshire et al., 2009b) these effects were greatly reduced by replacing the aircraft's standard nadir window with two wedged and AR coated windows.

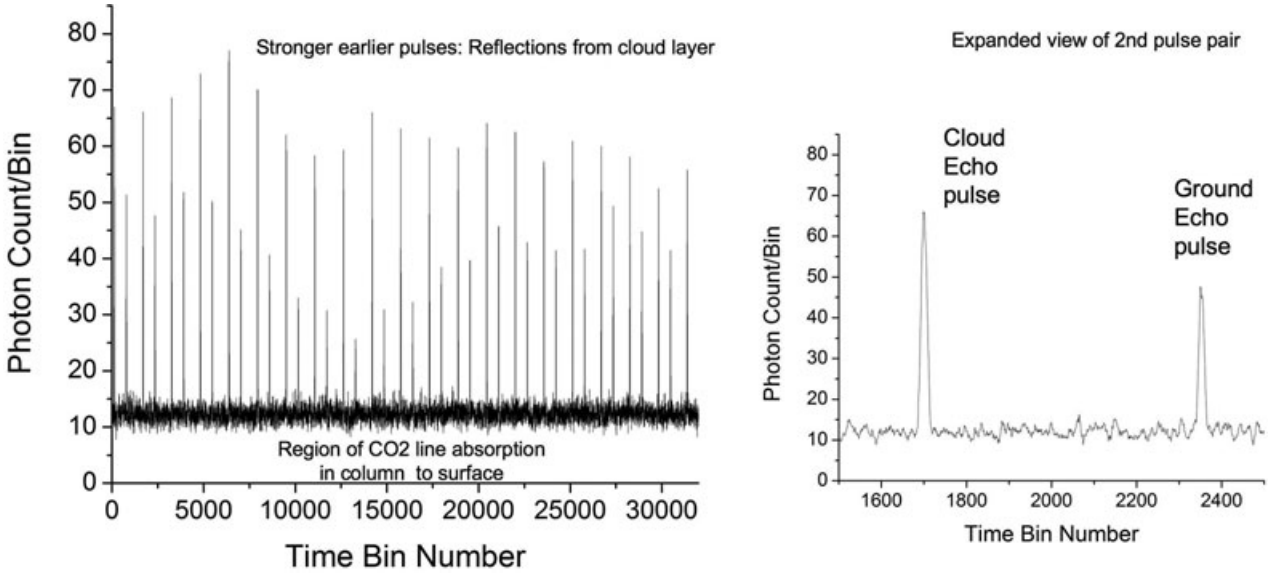

Fig. 7. Left panel: Example of a time resolved airborne measurement through a thin cloud deck, made from 7.2 km altitude with 20 wavelength steps across the CO_2 line. The integration time was 1 s and the measurement time resolution was 64 ns bin^{-1} (9.6 m bin^{-1}), with 16 bins pulse^{-1}. For clarity the plot used an eight bin running average. For each group the first pulse is from cloud and second pulse is from the surface. The cloud to ground distance is ∼6.2 km. The received energy of the surface reflected pulses show the attenuation from CO_2 line absorption, with a transmission minimum at approximately bin 12500. This measurement is not corrected for wavelength variability (etalon fringes) caused by the aircraft's nadir window. Right panel: Expanded view of the second pulse pair.

8. Airborne CO_2 measurements and calculations

Airborne CO_2 column measurements were made from flights on December 7, 2008 above Department of Energy (DOE) Southern Great Plains ARM (Atmospheric Radiation Measurements) site near Lamont Oklahoma. There were two 2-h long flights, one in the early afternoon and one in the evening. Lidar measurements were made at stepped flight altitudes from 1.5 to 7 km. The flight patterns are shown in Fig. 8 where the length of the straight-line segments were ∼32 km. The patterns were flown with three segments at constant altitude, and the altitude was stepped, upward or downward, during the eastern-most segment. The lidar functioned well during the flights and a plot of a detected single off-line wavelength signal count versus altitude measured over several flights is shown in Fig. 9. The received signal levels followed the R^{-2} dependence predicted by eq. (1), with about 1500 detected counts s^{-1} for an off-line wavelength at 8 km altitude. The daytime detected solar background count rate was about 550 KHz. For 1 s averaging time the noise counts per laser pulse were about 250 counts, which is consistent with values predicted by eq. (2). At 8 km altitude the SNR for an off-line wavelength was ∼33 for a 1 s averaging time, and the relative error in the received energy estimate was ∼3%.

For the experiments above the DOE ARM site, the land surface was wintertime prairie and was fairly uniform in reflectivity. However if the surface reflectivity viewed by the moving lidar varies rapidly (i.e. at a significant fraction of the 450 Hz line scan rate), the changing reflectivity may introduce some residual variability in the average detected signal energy and in the line shape measurement. Hence the spatial variability in reflectivity along the flight track, the wavelength scan rate and degree of footprint overlap on the ground can be important (Amediek et al., 2009). Some calculations for this experiment are summarized in Table 2. They show the Lear-25 speed increases modestly with altitude, and with a fixed laser divergence, the laser spot diameter on the ground increases linearly with altitude. For these flights the aircraft travelled ∼32 cm per line scan. The laser footprint areas for the middle half of the scans were ∼64% overlapped at 2.44 km altitude, and the fraction increased to 84% at 7.1 km. Hence this experiment was most sensitive to any rapid (m-scale) surface reflectance changes at lower altitudes. With the fairly uniform surface reflectivity for these experiments, the signal variability due to any reflectance changes was small, and was almost always less than the single pulse SNR from the signal shot noise. Due to their increasing diameters on the surface, the laser spots are more overlapped at higher altitudes, such as those made in 2009, and so their sensitivity to reflectivity changes is smaller.

In order to estimate the actual CO_2 column density, measurements of atmospheric temperature, moisture and pressure vertical profiles were used from the DOE radiosonde balloons, which were launched from Lamont, OK every 6 h. Their parameters were used in a 40 layer atmospheric model to compute dry

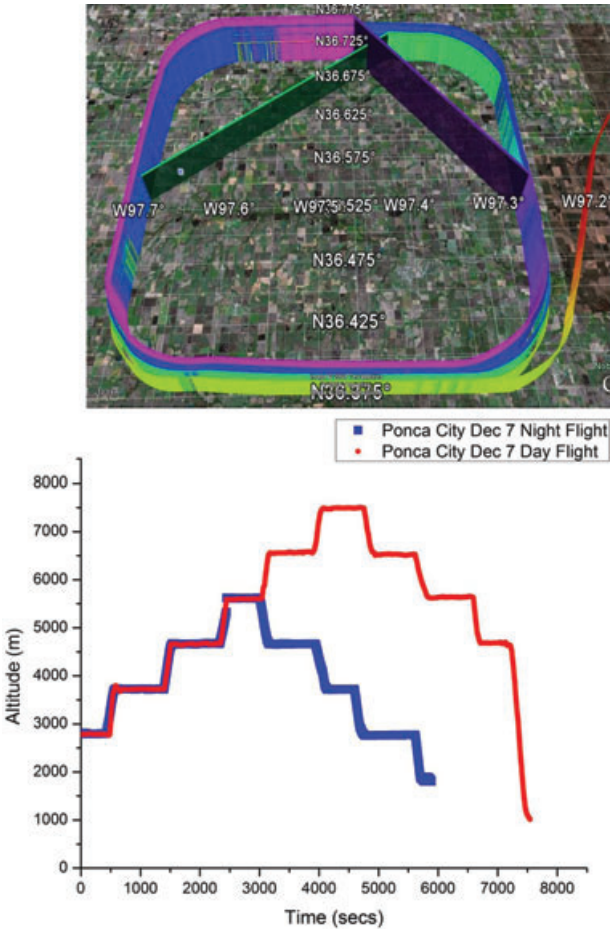

Fig. 8. The airborne flight pattern for the two flights above the DOE ARM site near Lamont Oklahoma on December 7, 2008. Upper panel: a map of the flight patterns, which were flown in a counterclockwise direction. The radiosonde site at Lamont, OK (97.48°W, 36.62°N) is in the middle of the pattern (source: Google Earth). Lower panel: the altitude profiles versus time for both flights. For each flight rotation three segments were flown at constant altitude and the eastern most leg was used to change altitude.

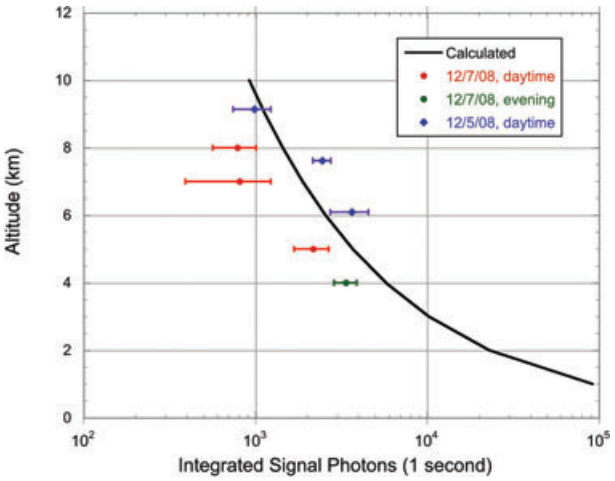

Fig. 9. Symbols: the measured lidar detected signal photon counts for a single off-line wavelength and 1 s integration times at different flight altitudes for three flights during December 2008. Solid line: predicted signal levels from calculations using eq. (1).

Table 2. Airborne Surface Sampling vs Altitude and Aircraft Speed

Altitude (km)	2.44	5.3	7.15
Nominal Lear speed (m/sec)	133	162	175
Receiver FOV diameter on ground (m)	0.3	1.06	1.43
Lear forward motion during 1 scan (m)	0.27	0.32	0.35
Receiver FOV fraction moved per CO_2 line scan (%)	89	30	24
Spot overlap fraction for middle 50% of scan (%)	64	81	84

air column density versus height to 8 km altitude. The December 7th airborne flights were also coordinated with DOE investigators. They used a small single engine Cessna aircraft carrying an in situ quick-response infrared absorption gas analyser to measure CO_2 concentrations. It sampled air and CO_2 concentrations every second from takeoff to ~6 km (its altitude limit) and back to the ground. Two Cessna flights were made on December 7, 2008, each lasting about 2 h, and their measurements provided vertical profiles of CO_2 mixing ratios.

Figure 10 shows the vertical profiles of CO_2 mixing ratio measured by the in situ analyser on both Cessna flights. The upward leg (black dots) was a direct ascent, but the descent measurements (blue dots) are flown in downward stepped pattern with 10 and 5 min long legs flown horizontally at every 305 m (1000 ft) altitude. The aircraft speed was about 50 m s^{-1} and the leg directions were approximately perpendicular to the wind speed. The spread of values in the descent measurements indicate the spatial variability of the CO_2 concentrations sampled at the altitude steps. This is especially noticeable at lower altitudes within the boundary layer, and for the second flight. Given this spatial variability, for this computation the simplified straightline approximations, shown in red, were used for the column density calculation. Figure 11 shows the two-way (aircraft-to-ground and back) optical depth and transmittance computed based on HITRAN 2004 and the Cessna and radiosonde measured conditions versus altitude for two adjacent 1572 nm lines, for the early afternoon flight on December 7, 2008. As expected the line transmittance decreased with increasing flight altitude and column length. Figure 12 shows the averaged two-way optical depth for the 1572.335 nm line and the CO_2 column number density plotted versus flight altitude. Both increase smoothly with height. These calculations provided a reference comparison for the airborne lidar measurements and showed how the CO_2 line shapes and depths should respond to flight altitude.

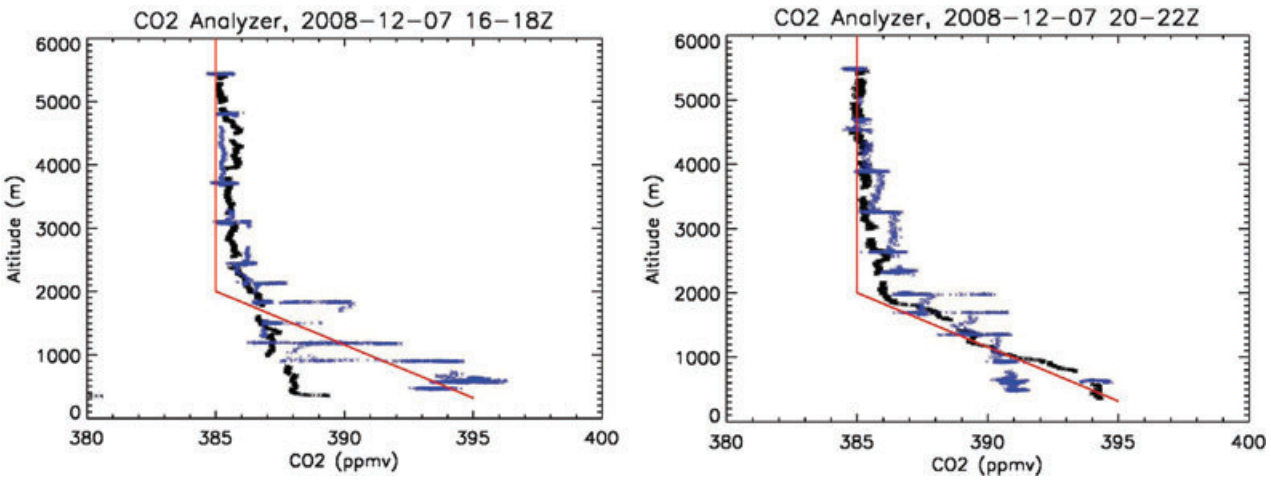

Fig. 10. In situ CO_2 concentrations versus altitude measured by the DOE Cessna aircraft with an infrared gas analyser. Left-hand profile is from a noon flight and the right-hand profile from a late afternoon flight on December 7, 2008. The black dots are measurements made during the aircraft's direct ascent, and the blue dots are those measured during the altitude-stepped decent, where the aircraft sampled CO_2 while flying horizontally for 5–10 min per altitude. The spread in blue dots at the altitude bands is caused by the spatial variability of CO_2 concentrations at the altitude. The red lines are the functions used to approximate the concentration profiles.

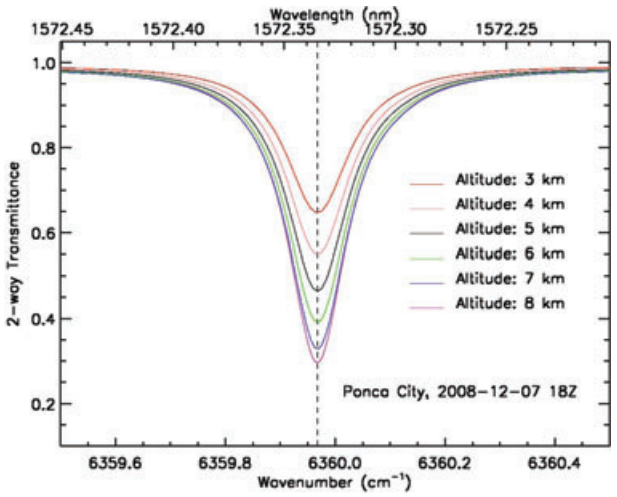

Fig. 11. The two-way optical transmittance of the 1572.335 nm CO_2 line as a function of flight altitude for December 7, 2008 computed from the radiosonde and Cessna readings.

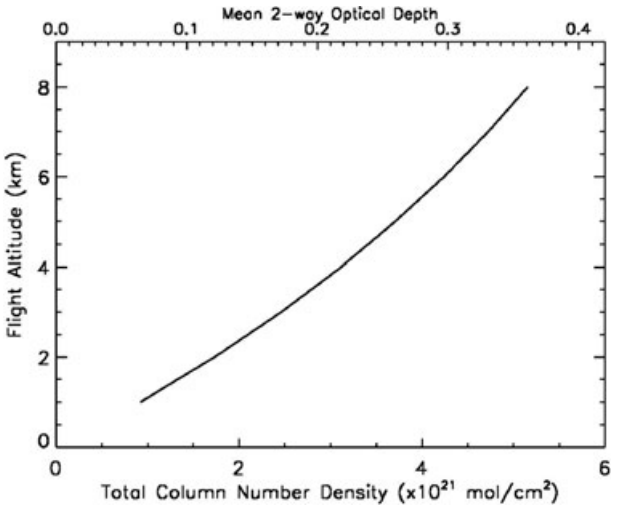

Fig. 12. The computed mean two-way optical depth (top scale) and number density (bottom scale) for the 1572.335 nm CO_2 line measured in the flights as a function of flight altitudes for the flights of December 7, 2008.

9. CO_2 measurement processing and line retrievals

For the flights above the ARM site, the lidar recorded the time- and wavelength-resolved laser backscatter with the photon counting timing system with 1 s integration time. In subsequent analysis, the measurements at each flight altitude step where averaged, using between 15 and 100 s of lidar measurements per altitude. We used a CO_2 line retrieval approach based on the Gauss–Newton method (Rodgers, 2000) to analyse the airborne line shape measurements. This approach has sufficient free parameters to model and correct for instrument effects, to fit the resulting CO_2 line shapes, and to estimate the corresponding CO_2 column densities (and mixing ratios) at each altitude. The CO_2 retrieval algorithm yields an estimate of the mean CO_2 concentration over the laser path length based on line absorption strength. The input observations were the ratio of the photon counts in the surface echo signals at each wavelength after they were normalized by an estimate of transmitted pulse energy. The error covariance matrix for the observed signals was diagonal and equally weighted for all but the last received wavelength.

The algorithm required several other fixed quantities as inputs. First is a vertical profile of temperature, pressure and water vapour content with altitude. This was estimated from gridded meteorological fields from the Goddard Modelling and Assimilation Office for Lamont OK on December 7, 2008 at the time of the flights. It uses the wavelength resolved absorption spectra of atmospheric CO_2 based upon HITRAN 2004. Finally, it used the path length from the aircraft to the surface, which was calculated from the laser pulse's time of flight to the surface. Based on both ground-based testing and subsequent airborne measurements, the range resolution for these flights was estimated to be ~5 m. Since this was 0.3–0.1% of the column height, for these flights its contribution to the overall CO_2 measurement error was negligible.

The algorithm fits the sampled CO_2 line shape using a model with several sets of variables. The first is the reduction of the photon count ratio near the 1572.335 nm line due to CO_2 absorption. Since the photon counts for the line shape samples are measured as a function of pulse number, they are converted to wavelength before comparing the observed spectra with the HITRAN data. For these experiments the lidar's wavelength (i.e. wavelength per laser pulse number) was modelled as a quadratic function, and the three wavelength coefficients were solved for, using the ground calibration as a prior constraint. The final set of variables modelled the changes in the lidar's baseline response, $E_{las}(\lambda)\tau_{opt}(\lambda)$, with wavelength. This product varied during flight due to wavelength dependent laser power and etalon fringe pattern in the aircraft's window transmission. For these experiments the dominant source of variability was a sinusoid in transmission caused the aircraft's nadir window. There were about 4 cycles per wavelength scan, which changed more considerably more rapidly with wavelength than did the CO_2 absorption. The phase of the etalon fringe pattern changed with time and window temperature. We modelled and normalized for an estimate of the baseline variability, $E_{las}(\lambda)\tau_{opt}(\lambda)$, by using a quadratic energy dependence with a simple sinusoidal etalon transmission model. For these flights 10 adjustable parameters were used to solve for the baseline variability and the three wavelength coefficients of the sweep function. To solve for the best-fitting line shape, the CO_2 concentration, the linear and polynomial coefficients were varied simultaneously to minimize the difference between the computed (modelled) photon count ratios and the measured ones. Since each lidar measurement provided the received energy counts for the 20 wavelengths, the algorithm's requirement for 10 inputs was considerably over determined. This permitted flexibility in line fitting and error determination. In subsequent flights (Abshire et al., 2009b) we used custom aircraft windows, which are both wedged and AR coated, and the etalon fringes and baseline variability were reduced by an order of magnitude.

An example of calculated and the observed (retrieved) line shapes for the flights over the ARM site are shown in Fig. 13. The retrieved line shapes have similar shape and altitude dependence as the calculated ones. However their shape is not as smooth. This indicates that for these experiments the lidar had some residual wavelength variability, which was not accurately modelled by the retrieval algorithm. The measurements at the lowest altitudes, with their smaller illuminated spot sizes, are more likely to be impacted by any variability in surface reflectivity, while the higher altitude measurements were made with fewer detected photons. The shape agreement was considered good, given the impact of the aircraft window's etalon effects and that these were the initial lidar flights.

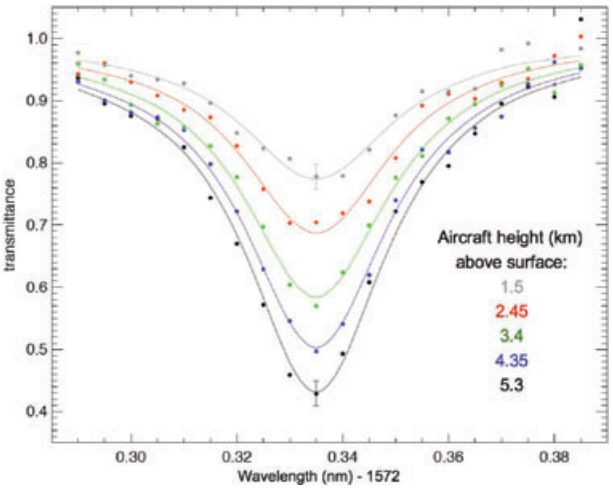

Fig. 13. Some CO_2 transmission line shapes versus altitude for flights, with altitudes colour coded in same way as indicated in insets. Solid lines: calculated shapes based on airborne in situ readings. Dots: lidar measured line shape after processing with CO_2 retrieval algorithm with estimated 1σ error bars.

The line shape fits were then used to compute the CO_2 column number density and, given the dry air column density estimate from the radiosonde, the mixing ratio. The results are shown in Fig. 14, along with the calculated values from the in situ measurements. The centre dots represent the mean of all the retrieved values (typically 20) for the altitude, and the individual retrievals were based on an average of 15 s of lidar measurements. The error bars are ± 1 standard deviation. The amount of CO_2 predicted from the lidar readings increased as expected with the laser path length (flight altitude) and were generally consistent with the in situ measurements. The average difference between the computed column densities and the 4 measurements between 4.3 and 7.1 km altitude was 2.5%, or equivalently 9.8 ppm. These are larger than the shot noise limit. The primary causes of variability in these initial measurements were the significant variability in the measured wavelength response caused by etalon fringing from the aircraft's window and incomplete calibration of the lidar's wavelength and receiver responses. These sources of error have since been greatly reduced. Some of the average difference between calculated number densities and the measurements may be from

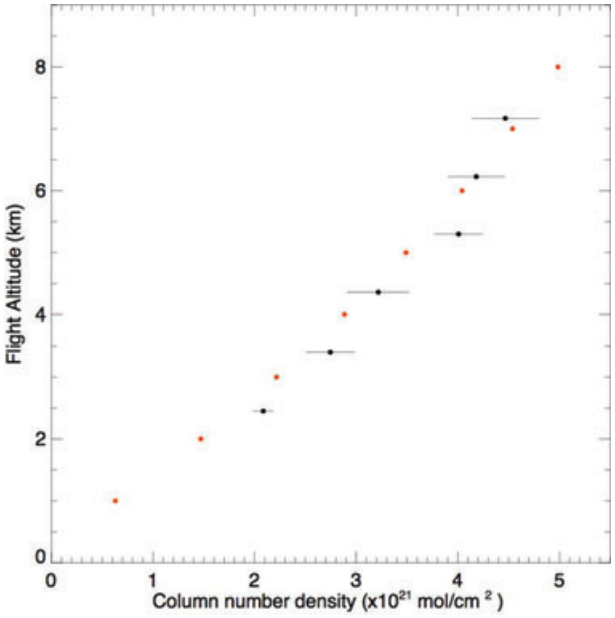

Fig. 14. Lidar estimated CO_2 column number density to surface with 1 standard deviation error bars (in black) made at the altitude steps versus the calculated CO_2 column density to surface (in orange) from the in situ sensor as a function of flight altitude.

errors in the HITRAN 2004 database for the 1572.335 nm CO_2 line.

10. Summary

We have demonstrated initial airborne measurements of CO_2 absorption and column abundance using a new pulsed direct detection lidar based on the IPDA technique. The lidar operates by scanning its laser wavelength across a CO_2 line near 1572 nm at a 450 Hz rate with 20 wavelength samples across the line. It measures the time resolved backscatter and absorption line shape in the column to the surface. Unlike previous airborne CO_2 lidar, it uses low energy (25 μJ) laser pulses and a sensitive photon counting PMT detector. A pulsed and time gated measurement approach is used to allow CO_2 column measurements through thin clouds.

Initial airborne lidar measurements were demonstrated during December 2008 and the lidar functioned well during flights between 3 and 11 km altitudes. Measurements were made using the 1572.335 nm CO_2 line in flights over the DOE ARM site including some through cirrus clouds. They showed clear absorption line shapes, which increased in optical depth with increasing aircraft altitude. CO_2 concentrations and dry air profiles made from radiosondes were used to estimate the column CO_2 number density, and expected line shapes were calculated using HITRAN 2004. The instrument's line shapes were estimated via a CO_2 line shape retrieval algorithm, which permitted solving and correcting for known instrument factors, including baseline offset, transmission variability, and the wavelength sweep parameters. The post-processed line shapes agreed well with those calculated from in situ measurements and radiosondes. The column number density versus altitude showed similar agreement with calculations, and the estimated CO_2 number density agreed within an average 2.5% for the higher altitudes. The limiting error sources for these initial flights were a significant variability in optical transmission versus wavelength caused by the aircraft's nadir window, instrument temperature changes and incomplete instrument calibration. These errors have since been reduced.

These initial airborne measurements have demonstrated a candidate lidar technique for CO_2 needed for the ASCENDS mission. In order to meet the ASCENDS measurement requirements, a lidar approach to measure the dry air column is needed, as well as improvements in calibration, precision, stability, readout rate and power scaling. In subsequent work, we have made several improvements to this airborne lidar. We have greatly reduced the variability in the instrument's wavelength response by replacing the aircraft window with ones both wedged and AR coated. We have improved the instrument's optical transmission, calibrations and receiver SNR. We have made additional flights during August 2009, to 13 km altitude, over various sites, and with additional measurements from in situ sensors (Abshire et al., 2009b). Those measurement results are being analysed and will be reported in the future.

11. Acknowledgments

We acknowledge the support of the NASA Earth Science Technology Office's Advanced Instrument Technology and Instrument Incubator Programs, the NASA Carbon Cycle Science Program, and the Goddard IRAD program. We appreciate the collaboration with the NASA Glenn Aircraft Operation office, and with Marc Fischer of Lawrence Berkeley Laboratory on the airborne in situ CO_2 measurements. We also appreciate the valuable work of other members of the Goddard CO_2 Sounder team, and the many suggestions from the reviewers.

References

Aben, I., Hasekamp, O. and Hartmann, W. 2007. Uncertainties in the space-based measurements of CO_2 columns due to scattering in the Earth's atmosphere. *J. Quant. Spectrosc. Radiat. Transfer.* **104**, 450–459.

Abshire, J. B., Collatz, G. J., Sun, X., Riris, H., Andrews, A. E. and co-authors. 2001. Laser sounder technique for remotely measuring atmospheric CO_2 concentrations. *EOS, Trans. Am. Geophys. Un.* **82**(47), Fall Meet. Suppl., Abstract GC32A-0221. Available from http://www.agu.org/meetings/ fm01/waisfm01.html.

Abshire, J. B., Riris, H., Sun, X., Krainak, M., Kawa, S. and co-authors. 2007. Lidar approach for measuring the CO_2 concentrations in the troposphere from space. In: *Proceedings of 2007 Conference on Lasers*

and Electro-Optics (CLEO-2007). Optical Society of America, Paper CThII5, ISBN: 978-1-55752-834-6.

Abshire, J. B., Riris, H., Hasselbrack, W., Allan, G., Weaver, C. and co-authors. 2009a. Airborne measurements of CO_2 column absorption using a pulsed wavelength-scanned laser sounder instrument. In: *Proceedings of 2009 Conference on Lasers and Electro-Optics (CLEO-2009)*. Optical Society of America, Paper CFU-2, ISBN: 978-1-55752-869-8.

Abshire, J. B., Riris, H., Allan G. R., Weaver, C., Hasselbrack, W. and co-authors. 2009b. Pulsed airborne lidar measurements of atmospheric CO_2 column absorption and line shapes from 3–13 km altitudes. *EOS, Trans. Am. Geophys. Un.* **90**(52), Fall Meet. Suppl., Abstract A34C-05. Available from http://www.agu.org/meetings/fm09/waisfm09.html.

Allan G. R., Riris, H., Abshire J. B., Sun X., Wilson E. and co-authors. 2008. Laser sounder for active remote sensing measurements of CO_2 concentrations. In: *Proceedings of the 2008 IEEE Aerospace Conference*. IEEE, Big Sky, MT. 1534–1540, doi:10.1109/AERO.2008.4526387.

Amediek, A. Fix, A., Wirth, M. and Ehret, G. 2008. Development of an OPO system at 1.57 μm for integrated path DIAL measurement of atmospheric carbon dioxide. *Appl. Phys. B* **92**, 295–302, doi:10.1007/s00340-008-3075-6.

Amediek, A., Fix, A. Ehret, G. Caron, J. and Durand, Y. 2009. Airborne lidar reflectance measurements at 1.57 um in support of the A-SCOPE mission for atmospheric CO_2. *Atmos. Meas. Tech. Discuss*. **2**, 1487–1536.

Browell, E. V., Dobler, J., Kooi, S., Choi, Y., Harrison, F. and co-authors. 2009. Airborne validation of active CO_2 LAS measurements. *EOS, Trans. Am. Geophys. Un.* **90**(52), Fall Meet. Suppl., Abstract A34C-04. Available from http://www.agu.org/meetings/fm09/waisfm09.html.

Caron, J. and Durand, Y., 2009. Operating wavelengths optimization for a spaceborne lidar measuring atmospheric CO_2. *Appl. Opt.* **48**, 5413–5422.

Dufour E. and Breon, F. M. 2003. Spaceborne estimate of atmospheric CO_2 column by use of the differential absorption method: error analysis. *Appl. Opt.* **42**, 3595–3609.

Durand, Y., Caron, J., Bensi, P., Ingmann, P., Bézy, J. and co-authors. 2009. A-SCOPE: concepts for an ESA mission to measure CO_2 from space with a lidar. In: *Proceedings of the 8th International Symposium on Tropospheric Profiling,* Delft University of Technology, the Netherlands, ISBN 978-90-6960-233-2.

Ehret, G., Kiemle, C., Wirth, M., Amediek, A., Fix, A. and co-authors. 2008. Space-borne remote sensing of CO_2, CH_4, and N_2O by integrated path differential absorption lidar: a sensitivity analysis. *Appl. Phys. B* **90**, 593–608, doi:10.1007/s00340-007-2892-3.

ESA A-SCOPE Mission Assessment Report. 2008. Available from http://esamultimedia.esa.int/docs/SP1313-1_ASCOPE.pdf. Accessed December 2009.

Fan, S., Gloor, M., Mahlman, J., Pacala, S., Sarmiento, J. and co-authors. 1998. A large terrestrial carbon sink in North America implied by atmospheric and oceanic carbon dioxide data and models. *Science* **282**, 442–446.

Gibert, F., Flamant, P. H., Bruneau, D. and Loth, C. 2006. Two-micrometer heterodyne differential absorption lidar measurements of the atmospheric CO_2 mixing ratio in the boundary layer. *Appl. Opt.* **45**(18), 4448–4458.

Gibert, F., Flamant, P. H. and Cuesta, J. 2008. Vertical 2-um heterodyne differential absorption lidar measurements of mean CO_2 mixing ratio in the troposphere. *J. Atmos. Ocean. Technol.* **25**, 1477–1497, doi:10.1175/2008JTECHA1070.1.

Hetch, E. 2000. *Optics*, second edition. Addison-Wesley, Reading, MA, USA.

Kameyama, S., Imaki, M., Hirano, Y., Ueno, S., Kawakami, S. and co-authors. 2009. Development of 1.6 um continuous-wave modulation hard-target differential absorption lidar system for CO_2 sensing. *Opt. Lett.* **34**(10), 1513–1516.

Kuang, Z., Margolis, J., Toon, G., Crisp D. and Yung, Y., 2002. Spaceborne measurements of atmospheric CO_2 by high-resolution NIR spectrometry of reflected sunlight: an introductory study. *Geophys. Res. Let.* **29**(15), 1716, doi:10.1029/2001GL014298.

Koch, G., Barnes, B. W., Petros, M., Beyon, J. Y., Amzajerdian, F. and co-authors. 2004. Coherent differential absorption lidar measurements of CO_2. *Appl. Opt.* **43**(26), 5092–5099.

Koch, G. J., Beyon, J. Y., Gibert, F., Barnes, B. W., Ismail, S. and co-authors. 2008. Side-line tunable laser transmitter for differential absorption lidar measurements of CO_2: design and application to atmospheric measurements. *Appl. Opt.* **47**(7), 944–956, doi:10.1364/AO.47.000944.

Krainak, M.A, Andrews, A. E., Allan, G. R., Burris, J. F., Riris, H. and co-authors. 2003. Measurements of atmospheric CO_2 over a horizontal path using a tunable-diode-laser and erbium-fiber-amplifier at 1572 nm. In: *Proceedings of the Conference on Lasers and Electro-Optics/Quantum Electronics and Laser Science Conference*. Technical Digest, Optical Society of America, paper CTuX4, 878–881, ISBN: 1-55752-748-2.

Mao, J. and Kawa, S. R. 2004. Sensitivity Study for Space-based Measurement of Atmospheric Total Column Carbon Dioxide by Reflected Sunlight. *Appl. Opt.* **43**, 914–927.

Mao, J., Kawa, S. R., Abshire, J. B. and Riris, H. 2007. Sensitivity studies for a space-based CO_2 laser sounder. *EOS, Trans. Am. Geophys. Un.* **88**(52). Fall Meet. Suppl., Abstract A13D-1500.

Measures, R., 1992. *Laser Remote Sensing: Fundamentals and Applications*. Krieger Publishing Company, New York.

NASA ASCENDS Mission Science Definition and Planning Workshop Report. 2008. Available from: http://cce.nasa.gov/ascends/12-30-08%20ASCENDS_Workshop_Report%20clean.pdf. Accessed December 2009.

NASA-Glenn. 2010. Available from: http://www.grc.nasa.gov/WWW/AircraftOps/Learjet.html. Accessed December 2009.

O'Brien D. M. and Rayner, P. J. 2002. Global observations of carbon budget 2, CO_2 concentrations from differential absorption of reflected sunlight in the 1.61 um band of CO_2. *J. Geophys. Res.* **107**, 4354, doi:10.1029/2001JD000617.

Phillips, M. W., Ranson, J., Spiers, G. D. and Menzies, R. T. 2004. Development of a coherent laser transceiver for the NASA CO_2 laser absorption spectrometer instrument. In: *Proceedings of 2004 Conference on Lasers and Electro-Optics (CLEO-2004)*, Optical Society of America, Paper CMDD2.

Riris, H., Abshire, J., Allan, G., Burris, J., Chen, J. and co-authors.2007. A laser sounder for measuring atmospheric trace gases from space. *Proc. SPIE* **6750**, 67500U, doi:10.1117/12.737607.

Rodgers, C. 2000. *Inverse Methods for Atmospheric Soundings, Theory and Practice*. Volume 2, Series on Atmospheric, Oceanic and Planetary Physics, World Scientific, 238.

Sakaizawa, D., Nagasawa, C., Nagai, T., Abo, M., Shibata, Y. and co-authors. 2009. Development of a 1.6 μm differential absorption lidar with a quasi-phase-matching optical parametric oscillator and photon-counting detector for the vertical CO_2 profile. *Appl. Opt.* **48**(4), 748–757.

Stephen, M., Krainak, M., Riris H. and Allan, G. R. 2007. Narrowband, tunable, frequency-doubled, erbium-doped fiber-amplifed transmitter. *Opt. Lett.* **32**(15), 2073–2076.

Stephen, M. A., Mao, J., Abshire, J. B., Kawa, S. R., Sun X. and co-authors. 2008. Oxygen spectroscopy laser sounding instrument for remote sensing of atmospheric pressure. *IEEE Aerospace Conf.* 1–6, doi:10.1109/AERO.2008.4526388.

Tans, P. P., Fung, I. Y. and Takahashi, T. 1990. Observational constraints on the global atmospheric CO_2 budget. *Science* **247**, 1431–1438.

Tsai, B.-M. and Gardner, C. S. 1985. Time-resolved speckle effects on the estimation of laser-pulse arrival times. *J. Opt. Soc. Am. A* **2**, 649–656.

Uchino, O. and co-authors. 2009. Initial validation of GOSAT standard products. In: *Proceedings of the 8th Internaitonal Carbon Conference*, Jena, Germany, September 13–19.

United States National Research Council. 2007. Earth science and applications from space: national imperatives for the next decade and beyond. Available from http://www.nap.edu/. Accessed December 2009.

Weitkamp, C. 2005. *Lidar: Range Resolved Optical Remote Sensing of the Atmosphere*. Springer, Berlin, Heidelberg, New York.

Werle, P., Mucke, R. and Slemr, F. 1993. The limits of signal averaging in atmospheric trace-gas monitoring by Tunable Diode-Laser Absorption Spectroscopy (TDLAS). *Appl. Phys. B* **57**, 131–139.

Werle P., Mazzinghi, P., D'Amato, F., De Rosa, M., Maurer, K. and co-authors. 2004. Signal processing and calibration procedures for in situ diode-laser absorption spectroscopy. *Spectrochim. Acta Part A* **60**, 1685–1705.

Yokota, T., Oguma, H., Morino, I., Higurashi, A., Aoki, T. and co-authors. 2004. Test measurements by a BBM of the nadir-looking SWIR FTS aboard GOSAT to monitor CO_2 column density from space. *Proc. SPIE.* **5652**, 182, doi:10.1117/12.578497.